

CEBAF PROPOSAL COVER SHEET

This Proposal must be mailed to:

CEBAF
Scientific Director's Office
12000 Jefferson Avenue
Newport News, VA 23606

see letter attached

and received on or before OCTOBER 30, 1989

A. TITLE:

An Experiment to Measure The Charge Form Factor of The Neutron

B. CONTACT PERSON:

Donal Day

ADDRESS, PHONE AND BITNET:

University of Virginia
504 934 6566 DBD@VIRGINIA

C. THIS PROPOSAL IS BASED ON A PREVIOUSLY SUBMITTED LETTER OF INTENT

YES
 NO

IF YES, TITLE OF PREVIOUSLY SUBMITTED LETTER OF INTENT

SAME

D. ATTACH A SEPARATE PAGE LISTING ALL COLLABORATION MEMBERS AND THEIR INSTITUTIONS

TITLE PAGE

=====

(CEBAF USE ONLY)

Letter Received 10-31-89

Log Number Assigned PR-89-018

By KES

contact: Day

CEBAF PROPOSAL

An Experiment to Measure the Charge Form Factor of the Neutron

D. Day (Spokesperson), R. Ent, R. Lindgren,
R. Lourie, R. Marshall, J. S. McCarthy,
R. Minehart, J. Mitchell, D. Počanić,
O. Rondon-Aramayo, and C. Smith,
Institute of Nuclear and Particle Physics
Department of Physics, University of Virginia
Charlottesville, VA 22901, USA

J. Jourdan, G. Masson and I. Sick
Institut für Physik, Universität Basel, CH-4056, Basel, Schweiz

J. Lichtenstadt
Department of Physics
Tel Aviv University, Tel Aviv, Israel

October 30, 1989

1 Introduction

The form factors of the proton and neutron are fundamental properties of the nucleon, and a critical testing ground for models based on QCD. A detailed knowledge of these quantities is essential to our understanding of the electromagnetic response functions of nuclei.

Our present knowledge of the neutron electric form factor is inadequate. The slope of $G_{En}(Q^2)$ at $q^2 = 0$ is accurately known from neutron-electron scattering. At higher Q^2 systematic errors are very large. There, G_{En} has been extracted from elastic $e-d$ scattering, or inclusive quasielastic $e-d$ scattering. In both cases removal of the proton contribution requires information about the deuteron structure and large uncertainties are introduced. Uncertainties in the theoretical description of the deuteron (mostly from FSI and MEC contributions) have especially negative consequences. As a result, G_{En} , until very recently, was known with a systematic error of about $\pm 100\%$. A new experiment at SACLAY[1] on $e-d$ elastic scattering has improved the situation at $Q^2 < 0.8$; the resulting systematic errors are $\simeq 30\%$. Serious doubts remain as a great deal of theoretical input on non-relativistic deuteron structure, relativistic effects and MEC are needed to infer G_{En} from elastic $e-d$ data. Figure 1 shows the best fits to the inferred G_{En} obtained by different models for the N-N interaction necessary to compute the deuteron structure. Such uncertainties and ambiguities are unsatisfactory for a quantity as fundamental as G_{En} . With the experiment proposed here we will be able to determine G_{En} without large theoretical corrections.

The large systematic errors in the past experiments result from two difficulties.

- For elastic e-d scattering the deuteron structure is very important: Accounting for it introduces errors which are magnified with the subsequent subtraction of the dominant proton contribution.
- For quasielastic e-d scattering, the longitudinal/transverse Rosenbluth separation introduces large systematic errors for the small term (charge). Furthermore the necessary subtraction of the dominant proton contribution increases the large systematic errors.

To improve this situation we need to study a reaction which is insensitive to the deuteron structure, which avoids a subtraction of the proton contribution and which avoids longitudinal/transverse Rosenbluth separation.

In this proposal we describe in detail an alternative way of extracting the Sachs Coulomb form factor G_{En} , by measuring the spin-dependent part of the elastic $e-n$ cross section. To this effect, we plan to detect quasi-elastically scattered electrons from a longitudinally polarized beam incident on polarized deuterium nuclei in deuterated ammonia (ND_3). The determination of the asymmetry in the cross section for two opposite orientations of either polarization, yields the product $G_{En} \cdot G_{Mn}$. In the remainder of the proposal we will review the exact relation

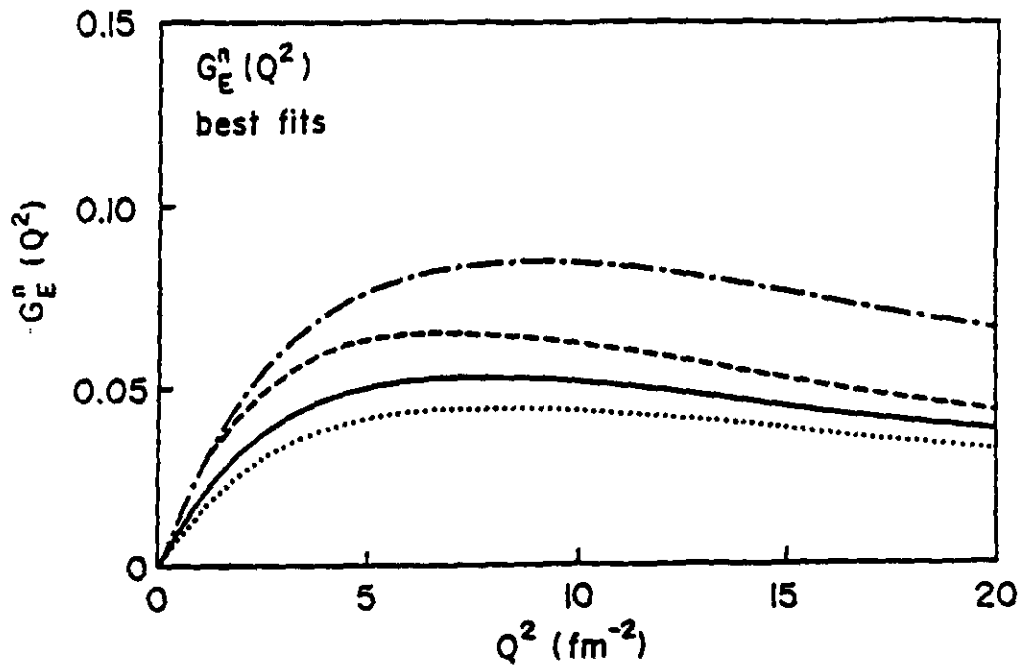


Figure 1: Two parameter fits to data for G_{eN} deduced from the Paris (solid), RSC (dotted), Argonne V14 (dashed) and Nijmegen (dash-dotted) potentials. From Reference [1].

between G_{E_n} and the experimental asymmetry, explore the kinematic region where the method may be applied, and discuss the technical details of the polarized target, the electron and the neutron detector systems, and the auxiliary devices involved. An analysis of the estimated uncertainties as well as a relation of the count rates and beam time request complete the proposal.

2 Proposed technique

Dombey[2] was the first to point out that the scattering of longitudinally polarized leptons on polarized nucleon targets could be used to determine the form factors of the nucleons. The procedure consists of measuring the part of the $e - N$ elastic cross section that corresponds to the interference between the Coulomb and the transverse components of the nucleon current. The measurement is carried out by calculating the resulting asymmetry in the cross section when the beam or the target polarization is reversed.

Following Donnelly and Raskin[3] we can express the inclusive $e - N$ cross section as a sum of an unpolarized part (Σ), that corresponds to the elastic cross section $d\sigma/d\Omega_e$, and a polarized part (Δ), that is different from zero only when the beam

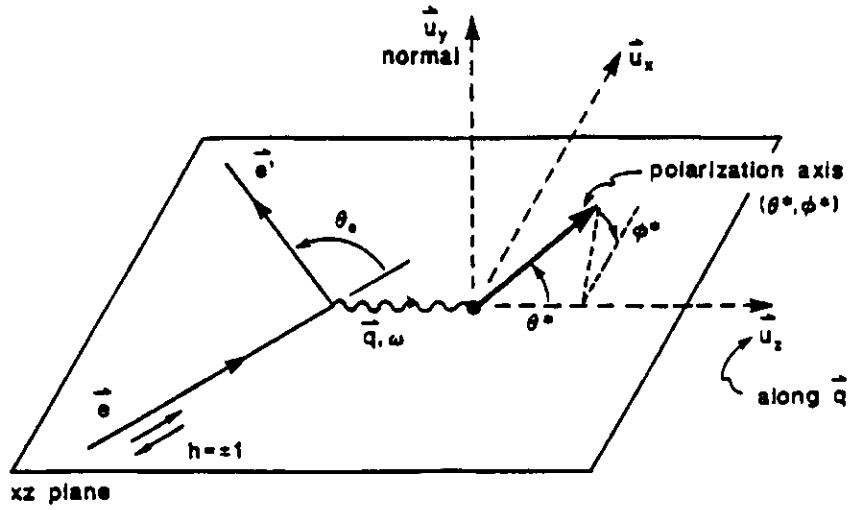


Figure 2: Coordinate system for $\vec{p}(\vec{e}, e')$ with orientation of polarization axis shown.

is longitudinally polarized (helicity h):¹

$$\sigma(h) = \Sigma + h\Delta; \quad h = \pm p_{beam}. \quad (1)$$

The asymmetry is then

$$A_n = \frac{\sigma(+)-\sigma(-)}{\sigma(+)+\sigma(-)} = \frac{\Delta}{\Sigma}. \quad (2)$$

As stated above, Σ is just the elastic unpolarized free $e - N$ cross section, and specifically for neutrons it reads

$$\Sigma = \sigma_{Mott} \frac{E'}{E_0} \left(\frac{G_{En}^2 + \tau G_{Mn}^2}{(1+\tau)} + 2\tau G_{Mn}^2 \tan^2(\theta_e/2) \right), \quad (3)$$

where $E_0(E')$ are the electron's initial (final) energy, $\tau = Q^2/4m_n^2$, m_n is the neutron mass, $-Q^2 = q_\mu^2$ is the square of the four-momentum transfer and $G_{E,Mn}$ are the neutron Coulomb and magnetic form factors. The polarized part Δ contains two terms, associated with the possible directions of the target polarization. The full expression is given below, with the kinematic factors and the nucleon form factors both evaluated in the laboratory frame (the elastic recoil factor f_{rec}^{-1} reduces to E'/E_0 in the extreme relativistic limit):

$$\Delta = -2\sigma_{Mott} \frac{E'}{E_0} \sqrt{\frac{\tau}{1+\tau}} \tan(\theta_e/2) * \left\{ \sqrt{\tau(1+(1+\tau)\tan^2(\theta_e/2))} \cos\theta^* G_{Mn}^2 + \sin\theta^* \cos\phi^* G_{En} G_{Mn} \right\} \quad (4)$$

where θ^* and ϕ^* are the laboratory angles of the target polarization vector with \vec{q} along the \vec{u}_z direction and \vec{u}_y normal to the electron scattering plane. It is clear

¹The longitudinal beam helicity is defined as parallel or opposite the beam momentum. See Figure 2 for the definition of the reference frame.

that to extract G_{En} the target has to be polarized longitudinally (i.e. $\phi^* = 0$) and perpendicular to \vec{q} ($\theta^* = \pi/2$). For this special condition, the asymmetry simplifies to

$$A_n = \frac{\Delta}{\Sigma} = \frac{-2\sqrt{\tau(1+\tau)}\tan(\theta_e/2)G_{En}G_{Mn}}{G_{En}^2 + \tau(1+2(1+\tau)\tan^2(\theta_e/2))G_{Mn}^2}. \quad (5)$$

This result was also obtained by Arnold *et al.*[4] who considered the measurement of the polarization of the recoil neutron, instead of using a polarized target.

The foregoing analysis is valid for free nucleons, and it has been reinterpreted in the case of neutrons in polarized nuclei. For the specific case of polarized deuterium nuclei, the exclusive process involving the detection of the neutron after the electrodisintegration can be similarly described[3] in an expression where the interference between G_{En} and G_{Mn} is contained in the polarized part.

The asymmetry for vector polarization of the deuteron in the orientation described above has been computed by Arenhövel *et al.*[5] for *s*-wave deuterons in the Born approximation, to be

$$A_{ed}^V = \sqrt{\frac{2}{3}}A_n, \quad (6)$$

where the $\sqrt{2/3}$ factor comes from the definition of the deuteron polarization.

There are different ways to exploit polarization observables for a determination of $G_E \cdot G_M$. One can either use a polarized beam and target as discussed above, or one can use a polarized beam and measure the polarization of the recoiling nucleon. In practice, the measurement using a polarized beam and target involves determining the experimental asymmetry

$$\epsilon = \frac{N_+ - N_-}{N_+ + N_-} = \frac{d^3\sigma(+)-d^3\sigma(-)}{d^3\sigma(+)+d^3\sigma(-)} = p_{beam}P_d^1A_{ed}^V, \quad (7)$$

which depends on the normalized numbers of counts for two opposite helicities, N_+ and N_- , therefore implying that the statistical uncertainty is the dominant one. The same expression obtains in the recoil polarimetry method, with the obvious reinterpretation of P_d^1 as the analyzing power of the polarimeter, A_x ; A_{ed}^V is then the polarization P'_z of the recoiling nucleon, and N_{\pm} are the numbers of counts in the up(down) segments of the polarimeter.

Our studies of these alternatives have led us to choose the polarized target technique. We have found that it allows us to measure G_E over a larger range of Q^2 than the alternative, and it avoids the difficult problem of a new calibration of the recoil polarimeter for every neutron energy (for every Q^2). In addition, the same setup (target and detectors) can be used to check the experimental technique and of the reaction mechanism, assumed to be quasi-free knockout by measuring G_{Ep} which is known over the Q^2 range we wish to study.

There are two different polarized targets which provide in effect polarized neutrons, polarized deuteron and polarized 3He . We have chosen polarized deuteron, as the theoretical description of the $(e, e'n)$ process is on a much firmer footing. For

the 2N-system the final state interaction can be treated exactly, while this is questionable for $A = 3$. The role of the D-state in the ground state wave function and the contributions of MEC, are under better control. Accurate calculations are already available, while for $A = 3$ we are still speculating on the size of the effects. At the same time, a deuteron target allows the experimental check on procedures and reaction mechanism through the comparison of the $d(e, e'n)$ and $d(e, e'p)$ reactions. Arenhövel *et al.*[5] have shown that, for the case of the deuteron, the uncertainties introduced by the deuteron structure are very small if one concentrates on the strength corresponding to quasielastic $e - n$ scattering with neutrons of small initial momentum, $k < k_f$. For such kinematic conditions and for the special case of the two-nucleon system, FSI can be accurately computed, and does not contribute significantly to the systematic errors. The effects of MEC, which for $A = 2$, also can be calculated with reasonable confidence, are small as well. Effects of both FSI and MEC are much smaller than the statistical and systematic errors of the experiment we propose.

To determine the region of Q^2 where the proposed technique may be most effective, the evaluation of a figure of merit (FOM) has become customary. In the present case, the figure of merit is related to the time required to accumulate the number of counts needed to determine the asymmetry to a given precision. This number is proportional to the product of the square of the asymmetry times the cross section, so the FOM is defined as

$$FOM = A_n^2 \frac{d\sigma}{d\Omega_e}.$$

Obviously, this quantity depends on the choice of a model for G_{En} .

Several models have been tried to describe the existing data, which extend, from the photon point to $Q^2 \cong 0.8[\text{GeV}/c]^2$. Among those deserving special attention are the so-called "dipole" model which uses the form $G_{En} = -\tau G_{Mn} = -\tau \mu_n G_{Ep}$, with $G_{Ep} = (1 + Q^2/0.71)^{-2}$, in fact setting the Dirac form factor F_{1n} to zero, in the full expression for the Sachs form factor $G_{En} = F_{1n} - \tau F_{2n}$; the phenomenological parameterization of Galster *et al.*[6], $G_{En} = -\tau G_{Mn}/(1 + p\tau)$; and the models that seek a connection between the value of the form factors at low momentum transfer and the asymptotic values of the Dirac and Pauli form factors F_{1n} and F_{2n} predicted by perturbative QCD, in particular the one proposed by Gari and Krümpelmann[7].

In Figure 3 we present the Q^2 dependence of G_{En} in those three instances. It can be seen that the dipole model is higher than the two others, and in fact it is an upper bound to the experimental data. On the other hand, the Galster parameterization (with the Feshbach-Lomon potential) gives a good fit for $p = 5.6$. We used these two models, which cover a broad range of possible values for the Q^2 dependence of G_{En} , to compute the FOM's, which are displayed in Figure 4. It is clear that the scattered electron angle θ_e has to be as forward as possible, while for a given θ_e , the FOM drops by a factor of ~ 100 (depending on the model) from its maximum value, when $Q^2 = 2.0[\text{GeV}/c]^2$. This places a practical limit on the upper value of the

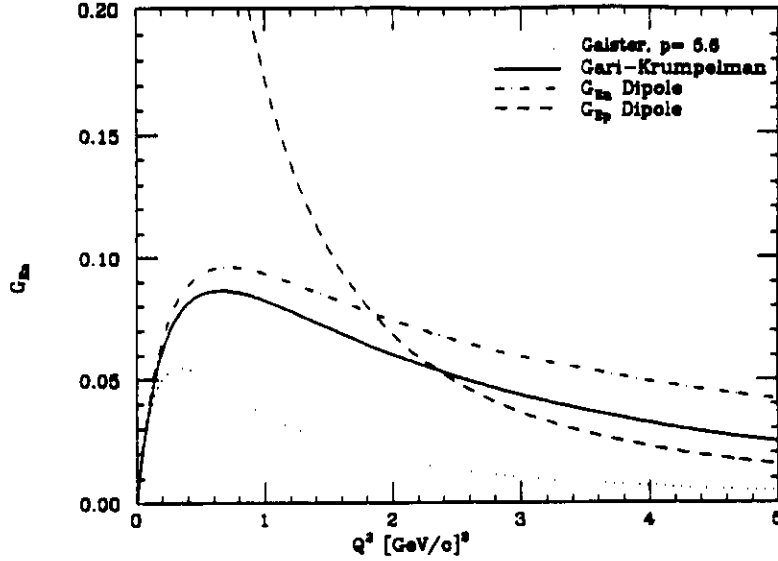


Figure 3: Q^2 dependence of G_{eN} for three different models.

attainable momentum transfer, independent of other technical complications that arise from the high kinetic energy of the recoil neutrons, and the opening of inelastic ($e, e'\pi$) and ($n, p\pi$) channels. Therefore, in the present experiment, we will attempt to extract $G_{E\pi}$ at four values of Q^2 , starting at about $0.5[\text{GeV}/c]^2$, up to $2.0[\text{GeV}/c]^2$.

To obtain these values of the four-momentum transfer, a combination of beam energies and scattering angles must be chosen so as to maximize the FOM, within the constraints of the CEBAF experimental halls, such as:

- Beam energy $\leq 4.0[\text{GeV}]$ ($\leq 6.0[\text{GeV}]$ in Hall C).
- Forward spectrometer angle $\simeq 15^\circ$.
- Electron final momentum in the range $0.5[\text{GeV}/c]$ to $4.0[\text{GeV}/c]$ ($6.0[\text{GeV}/c]$ in Hall C).

The table below gives a summary of the relevant quantities:

Table 1. Kinematic quantities

Q^2 [GeV/c] ²	E_0 [GeV]	ν_{qe} [GeV]	$ \vec{q} $ [GeV/c]	θ_e	θ_q	θ_B	T'_n [MeV]
0.5	2.849	0.273	0.758	15°	61.6°	28.4°	268
1.0	3.880	0.553	1.143	16°	53.3°	36.7°	540
1.5	3.973	0.843	1.487	20°	46.0°	44.0°	819
2.0	4.020	1.142	1.818	24°	40.1°	49.9°	1107

The symbols in this table have been defined earlier, with the exception of ν_{qe} which is the electron energy loss at the quasielastic peak, including the average

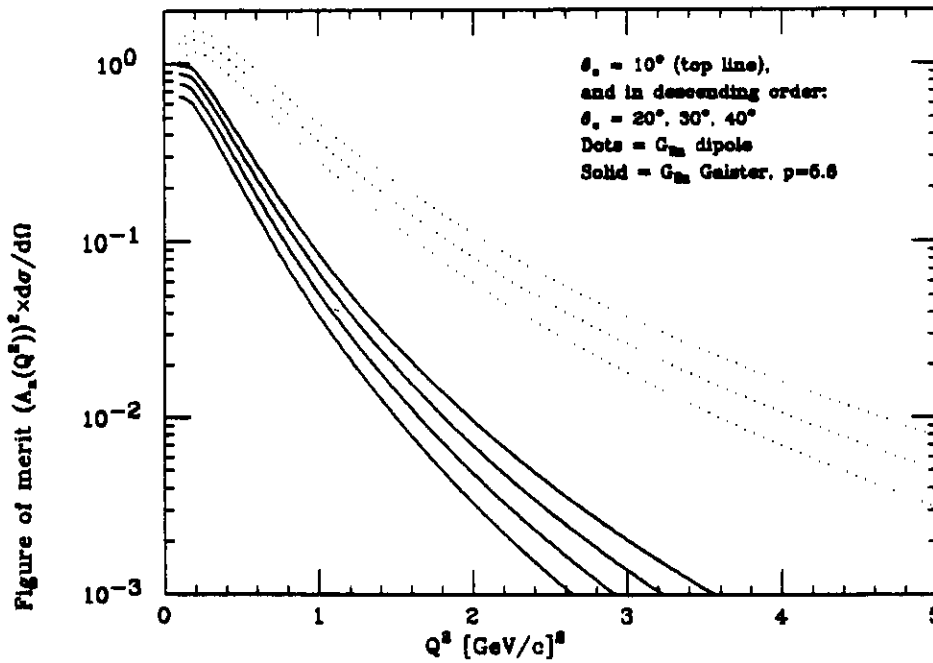
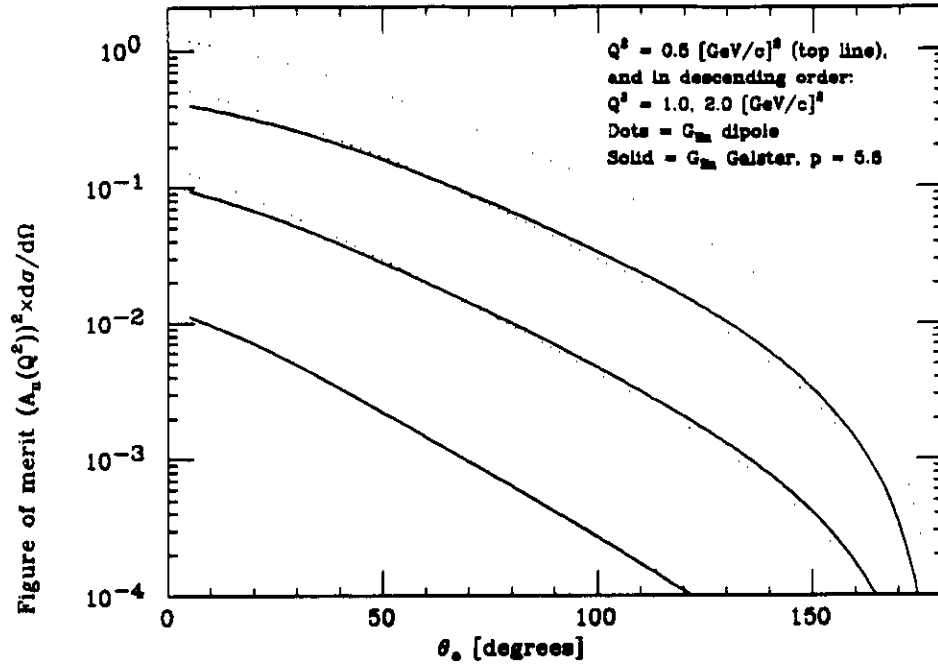


Figure 4: A(top) and B(bottom) display the figure of merit $A_n^2(d\sigma/d\Omega_e)$ for two models of G_{E_n} consistent with the existing experimental data at low and intermediate Q^2 , namely the dipole and Galster's parameterization with $p=5.6$, versus θ_e and Q^2 , respectively. The FOM are calculated for 4 angles with the Galster parameterization (10° , 20° , 30° , and 40°).

separation energy of the nucleon; θ_B which is the direction of the target magnetic field relative to the beam in the laboratory reference frame (main coordinate system), and is perpendicular to \vec{q} , corresponding to the values $\theta^* = \pi/2$, $\phi^* = 0$; and T'_n is the kinetic energy of the recoil neutrons in parallel kinematics (i.e. zero initial momentum).

The theoretical studies performed indicate clearly that $\vec{d}(\vec{e}, e'n)p$ will provide a clean determination of G_{En} with small systematic errors. This is an important criterion given the fact that past attempts to measure G_{En} were all limited by systematic errors in both experiment and, even more so, in the theoretical input necessary to infer G_{En} .

3 Simultaneous check of G_{Ep} through $\vec{d}(\vec{e}, e'p)$

Both the experimental procedures and our understanding of the reaction mechanism, can be checked by measuring with an identical setup used for $\vec{d}(\vec{e}, e'n)$ the reaction $\vec{d}(\vec{e}, e'p)$. At transfers $Q^2 < 1(\text{GeV}/c)^2$ the proton electric form factor is quite well known, and $\vec{d}(\vec{e}, e'p)$ can be used to verify those results.

A $\vec{d}(\vec{e}, e'p)$ experiment is much easier than $\vec{d}(\vec{e}, e'n)$: the $e - p$ cross section is much larger, the interference term $G_{Ep} \cdot G_{Mp}$ is much larger due to the larger G_{Ep} , and the detection efficiency for the recoiling nucleon is large. Typically, the figure of merit for $\vec{d}(\vec{e}, e'p)$ is two orders of magnitude greater than $\vec{d}(\vec{e}, e'n)$. Runs on $\vec{d}(\vec{e}, e'p)$ therefore are very short, or can be performed in parallel to $\vec{d}(\vec{e}, e'n)$ with a proton detector of much smaller size.

A $\vec{d}(\vec{e}, e'p)$ experiment is somewhat complicated by the fact that the proton exits the target in a direction nearly perpendicular to the holding magnetic field of the polarized target. This results in a significant vertical deflection of the proton, by up to 20° . This deflection does not pose significant problems. A (small) recoil proton detector can easily be placed out-of-plane for a simultaneous measurement of $(e, e'n)$ and $(e, e'p)$. Alternatively, a short run with the neutron detector (which does not need significant shielding) lifted out-of-plane can be performed.

To measure G_{Ep} with this setup, the proton detector be placed in direct sight of the target. Our experience with the $(e, e'n)$ experiment at NIKHEF shows that this is possible, provided the scintillators were shielded from the target with a few mm of Pb. For $Q^2 > 0.25 \text{ GeV}/c^2$ we have been able to run at NIKHEF with average currents of $\simeq 10 \text{ nA}$ and a duty cycle of 1%. We will be in a much more favorable situation at CEBAF, and even with a target that is significantly thicker than the LD_2 target employed at NIKHEF.

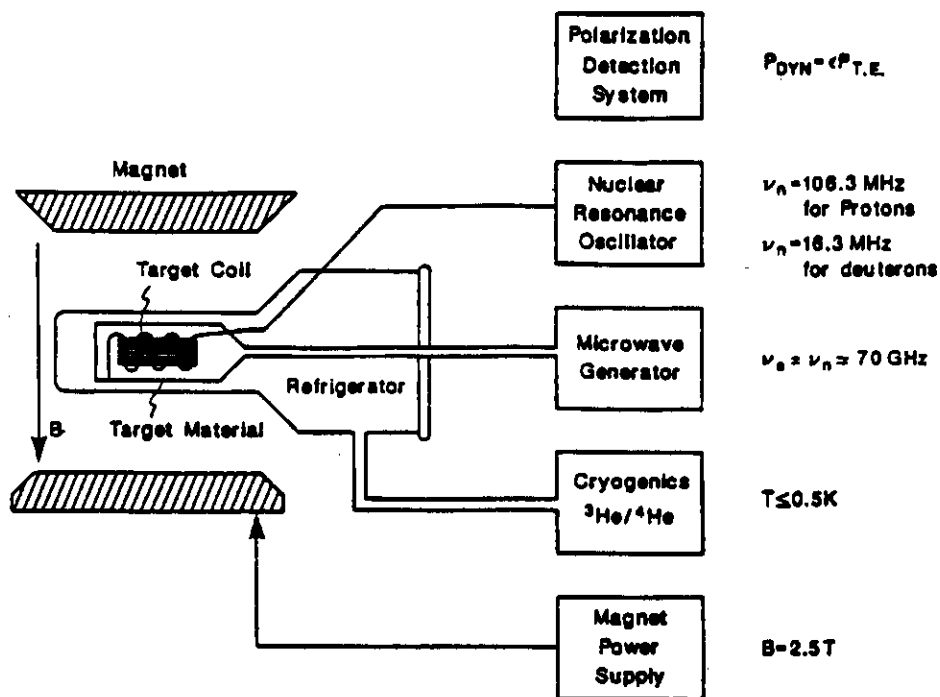


Figure 5: Schematic diagram of the main components of a polarized solid state target.

4 Experimental Setup

4.1 Polarized Target

There have been significant advances in the development of polarized solid state targets in the past few years[8]. The major breakthrough has been in the development of polarization in NH_3 and ND_3 , which have enhanced resistance to radiation damage and a higher percentage of polarized nucleons. The targets are polarized through the dynamic dipole-dipole interaction of the completely polarized radicals (electrons) and the nucleus. This requires very low temperatures ($\ll 1 \text{ K}$) and very high magnetic fields (2.5 - 5 Tesla). This large magnetic field is also of concern in the detection of scattered particles (see section dealing with the compensation of the holding field late in this proposal). The basic principle of operation is to cool the sample to low temperature ($< 1^\circ \text{ K}$) in a high magnetic field with RF power supplied to the sample. A schematic diagram of the major components is shown in Figure 5.

Some estimates have been made on the expected performance (see Table 2 below²) of the polarized targets in high power electron beams. These estimates

²The luminosity has been reduced to correspond to the percentage of polarized H and D.

are based upon existing systems, particularly the EMC apparatus used at CERN; the heat extraction from the target is the major limitation and will require not only a beam reduction, but a rapid movement (100 Hz) of the beam over the target area.

Table 2. Expected Polarized Target Performance.

Detail	NH ₃	ND ₃
Target Length	1.5 cm	1.5 cm
Temperature	1.0 K	0.2 K
Current	200 nA	10 nA
Luminosity	10 ³⁶	3 · 10 ³⁴
Vector Polarization	0.7	0.6
Tensor Polarization	—	0.3

The University of Virginia group is about to submit a proposal for the construction of polarized NH₃ and ND₃ targets. An initial compliment of equipment for this work has been acquired from funds supplied by the Commonwealth Center for Nuclear Physics; approximately \$125,000 has already been committed. The University is presently negotiating with a senior physicist with experience in spin physics to lead the target development effort.

Obviously this target is a general purpose facility for CEBAF, useful for many other experiments, including the *Deformation of the Δ* proposed by this collaboration. However, the primary motivation for undertaking the construction of the target is to measure G_{En} .

4.1.1 Compensation for Target Holding Field Effects

When using a polarized target, the holding field deflects all charged particles entering and exiting the target. For the $\vec{d}(\vec{e}, e'n)$ case of interest, the holding field is in the scattering plane, in the direction perpendicular to \vec{q} . The field has a component perpendicular to both the incident and scattered electron directions and results in small, yet significant deflections. This deflection of the electrons is minimized by performing the experiment at the highest incident energy (which corresponds to the smallest angle) possible, which, at the same time, yields the greatest the figure of merit for a fixed luminosity. For the energies and angles listed in Table 1, the maximum deflection for the incident electron in traversing a target field of 0.8 T-m is 2.8°. For the scattered electron the maximum deflection is less than 1.8°.

Unless compensated for the deflection of the incident and final electrons can be troublesome. When the beam is deflected down, the scattering plane is tilted such that \vec{q} points toward the floor. The angular position of \vec{q} below the laboratory floor, ϕ_q , is given by

$$\sin \phi_q = -\frac{E}{q} \sin \phi_b$$

where ϕ_b is the beam deflection angle. At high energies and small angles a small incident beam deflection is magnified, resulting in a large deflection of \vec{q} . For example, at $Q^2 = 0.5$, $\frac{E}{q} = 3.84$ and $\phi_q = 10.5^\circ$. Since the scattered electron is deflected

vertically as well, the scattering plane has a significant tilt with respect to the floor. To detect the neutron along \vec{q} 10 meters from the target would require putting the neutron detector almost 2 meters below horizontal. Further complications arise since the angle of the spectrometer, θ , is different from the true scattering angle when the beam is deflected. This difference between θ_e and θ , is greatest in the forward direction.

Therefore we have considered the possibility of compensating for the holding field. The following scenario has been investigated. The incoming electrons are bent vertically by a 2-magnet chicane. The holding field of the target brings them to the target center. The scattered electrons are bent vertically into the horizontal plane of the spectrometer. Since the target holding field bends vertically, electrons which are scattered with an out of (horizontal) plane angle of $\simeq 1.5^\circ$ arrive at the central plane of the spectrometer. This results in an scattering plane that is tilted with respect to the floor by only a degree.

The incident beam leaves the field of the target at small vertical angle, $\simeq 1.5^\circ$, and must be bent back to reach the beam dump, some meters away. Space for this chicane upstream of the target is available; no significant installation downstream that could interfere with the spectrometer is needed. This leaves the target polarization in the horizontal plane, and it does not require going out of the horizontal plane with the neutron detector (given the vertical acceptance angle of HMS).

The 2-magnet chicane needs to have a bending power of typically 1.4 T-m per magnet (2.8 T-m) with a pole gap of $\simeq 2$ cm to allow for beam rastering. For a pole width of $\simeq 8$ cm the range of angles needed for the range Q^2 can be covered. The resulting magnets are of modest size and pose minimal constraints in term of field quality. These magnets would be very similar (if not identical) to the ones used in the accelerator arcs.

The precession of the electron spin due to the effective beam deflection of $1-1.5^\circ$ before the target must be compensated at the polarized source.

4.2 Electron Spectrometer and Detection System

The HMS in Hall C or the HRS in Hall A have the necessary combination of momentum acceptance, resolution, and solid angle for this experiment. Only modest energy resolution on the electron side is necessary as the neutron arm dominates the overall determination of the missing energy. The large vertical acceptance of the these spectrometers is an advantage when considering the deflection of the electrons in the target field.

The detection package will consist of drift chambers for reconstruction of the electron angles and momenta; for particle identification, a gas Cerenkov counter and lead glass shower counters; and plastic scintillator hodoscopes for timing and to help with muon rejection in the shower counter. The needs of this experiment are well within the capabilities of the standard detection system planned for the CEBAF electron spectrometers. In fact, the low rates we anticipate, will not pose

a problem to their rate handling capabilities.

4.3 Beam Polarimetry

The polarization of high energy electrons can be measured by exploiting the asymmetry in electron electron scattering (Möller) and in the Compton scattering of circularly polarized laser from the polarized electrons in the incident beam. CE-BAF is planning to construct polarimeters of both types. For the high current halls the backscattered laser technique is feasible. However, since the maximum current handling capability of the solid state polarized targets is between 10 and 200 nA, it may not be possible to use this method for this experiment. The laser electron backscattering technique, which has a backscattering rate of 1 kHz/Watt/200 μ A[9], would produce very low scattering rates with potentially serious background problems at these currents.

The alternative is to use a Moller polarimeter which have been used successfully for low currents. Situated up stream of the target a Möller polarimeter consists of a polarized electron target, a septum magnet capable of deflecting the elastically scattered electrons into identical C-magnets located on opposite sides of the beam line. By detecting the incident electron and the scattered electrons in coincidence, which at the peak of the Möller asymmetry (90° in the CM) have one half of the incident beam energy, a nearly background free signal can be measured. The degree of polarization of the beam is measured by reversing the electron polarization, and for longitudinally polarized electrons a counting rate asymmetry is measured and compared to the expected experimental value of

$$A_{ee} = \frac{7}{9} \cdot P_e^B \cdot P_e^T$$

For polarized iron targets $P_e^T = 0.08$. The scattering rate will be about 10^5 Hz per 1μ A. Experience at existing laboratories (Bates, Bonn, Mainz) gives us confidence that the polarization of the beam can be determined to 3%.

4.4 Neutron Detector

Quasi-elastic scattering events from the neutron will be identified by detecting the recoil neutron in coincidence with the scattered electron. The neutron detector will consist of an array of scintillators which will form a continuous wall. The size of the neutron detector will be determined by two factors:

1. The solid angle required to match the electron spectrometer solid angle and contain the Fermi-broadened neutron peak corresponding to the quasi-elastic electron peak.
2. The neutron flight path necessary to obtain the required energy resolution to separate the 'quasi-elastic' recoiling neutron from background events.

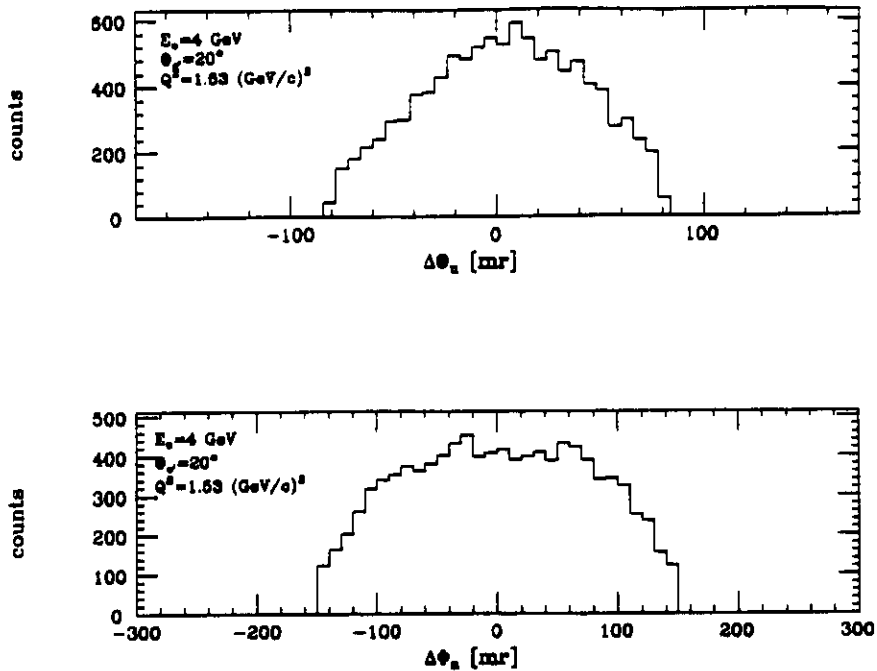


Figure 6: Neutron angular phase space at 4 GeV and 20° .

To determine the required solid angle which will match the electron spectrometer solid angle we performed a Monte Carlo calculation to simulate the quasielastic $d(e, e'n)p$ process. The neutron initial momentum was assumed to follow the nucleon momentum distribution in the deuteron. The spectrometer solid angle was assumed to be about 7 msr with a momentum bite acceptance of $\Delta p/p = \pm 10\%$. We show in Figure 6 the neutron angular phase space in the scattering plane ($\Delta\Theta_n$) and out of the scattering plane ($\Delta\Phi_n$) for an incident electron energy $E_e = 4$ GeV and electron scattering angle $\theta_e = 20^\circ$ corresponding to $Q^2 = 1.53(\text{GeV}/c)^2$. As can be seen in Figure 6, the recoil neutron peak is contained within $\Delta\Theta_n \approx \pm 80$ mr and $\Delta\Phi_n \approx \pm 150$ mr. Thus a neutron detector spanning 48 msr will contain most (85%) of the quasielastic peak.

There are three major sources of non-quasielastic, background ($e, e'n$) events;

1. Coincidence events originating from the nitrogen in the polarized target.
2. Charge exchange reactions (discussed later).
3. Coincidence events originating from the process $e + p \rightarrow e' + \pi + n$.

The first two can be determined by measuring the $N(e, e'n)$ reaction under the same conditions, or by a careful measurement of the nitrogen quasielastic peak (which extends beyond the deuteron peak) and subtracted from the deuteron quasielastic events (see Section 5).

To estimate the neutron energy resolution required to separate the quasielastic events from the π -production events we simulated by a Monte Carlo calculation

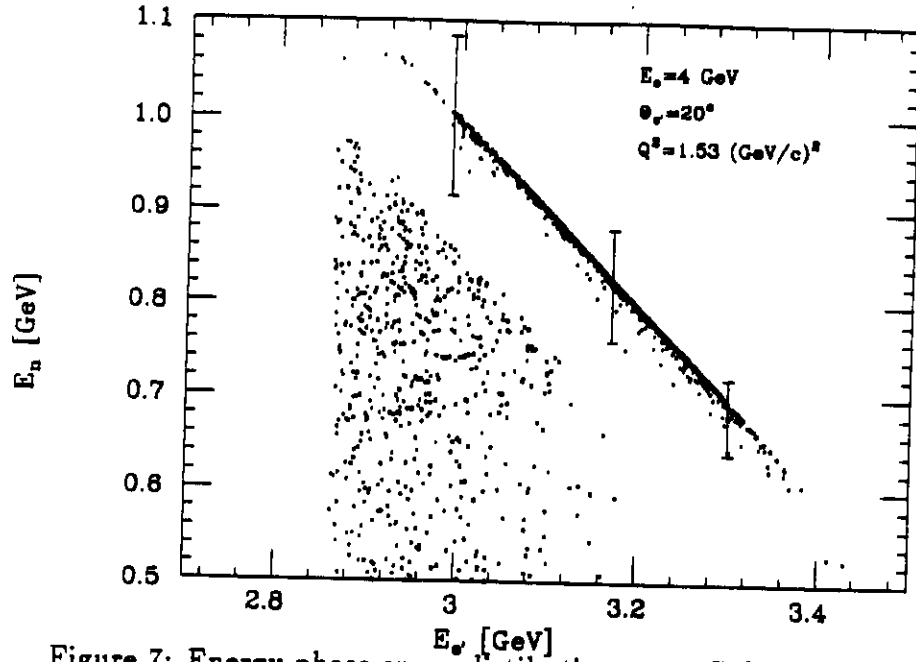


Figure 7: Energy phase space distributions at 4 GeV and 20°.

the energy phase spaces of the two processes. We show in Figure 7 the energy phase space distributions for both processes for the same kinematical conditions (for which the neutron kinetic energy is the highest in our proposed experiment and thus requires the longest flight path). The vertical bars in Figure 7 correspond to $\Delta E_n \approx 60$ MeV which can be obtained for this neutron kinetic energy (850 MeV) with a 10 m flight path and 0.5 ns timing resolution.

It should be noted that the quasielastic cross section is about equal to that of the π production cross section. However, while the neutron detector covers the entire quasi elastic phase space, only a fraction of the phase space of the neutrons originating from π -production processes will be covered by the neutron detector, thus eliminating the major part of the background. Using a Monte Carlo simulation, we estimated that the electron-neutron coincidence requirement with the given neutron detector will cut the double differential cross section to less than 5%, for events originating from either the deuteron or the nitrogen. For the ND_3 molecule, the effective coincidence e-n background cross section will be about 15% of the deuteron quasi-free background. The energy spectrum of these electrons is shown in Figure 8 with that of the quasi-free process. The smallness of this background ensures that the energy resolution obtainable with the neutron detector in this configuration should suffice to separate the deuteron quasielastic events from the π -production events. This is further demonstrated in Figure 9 where the energy spectrum of neutrons from the quasielastic and pion production processes in coincidence with electrons of $3.045 \leq E \leq 3.065$ GeV is shown. The horizontal bar represents the expected neutron energy resolution. The situation improves for events of higher scattered

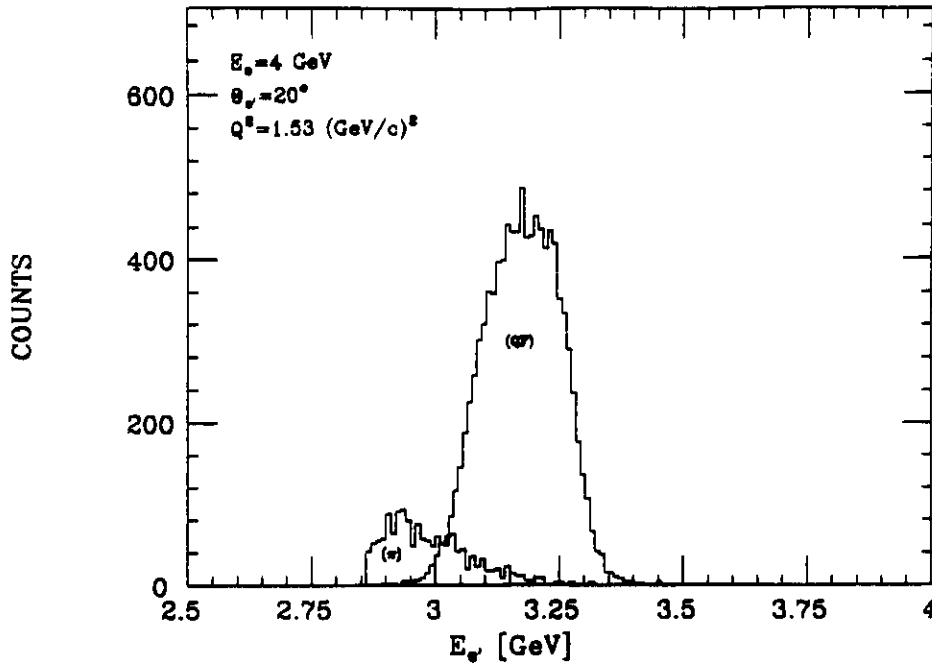


Figure 8: Electron energy spectrum for deuterium in coincidence with neutrons. The large peak is from quasielastic events, the small peak for reactions involving pions.

electron energy (toward the center of the quasielastic peak) where the neutrons are of lower energy.

The required neutron detector will be about $1.6 \times 3 \text{ m}^2$ in size. The detector will consist of $1.5 \times 0.1 \text{ m}^2$ scintillator bars 10 cm thick, a total thickness of 30 cm which will yield about 40% neutron detection efficiency. The University of Virginia is presently constructing a similar neutron detector $1.6 \times 1.6 \text{ m}^2$, 20 cm thick, with similar scintillating units. This detector will be redesigned for this experiment using the existing hardware (which comprises more than half of the required detector). The estimated cost for the additional hardware required for the neutron detector is \$300,000.

5 Corrections and Systematic Effects

5.1 Scattering from ^{14}N

Due to the limited energy resolution, $\simeq 60 \text{ MeV}$, it will not be possible to separate e-D and e-N quasielastic scattering via the missing energy in $(e, e'n)$. This does not pose a significant problem, however. Figure 10 shows a typical inclusive electron spectrum which reveals in the total spectrum the effect of the narrow deuteron quasielastic peak summed with the wider ^{14}N quasielastic peak. A cut on scattered

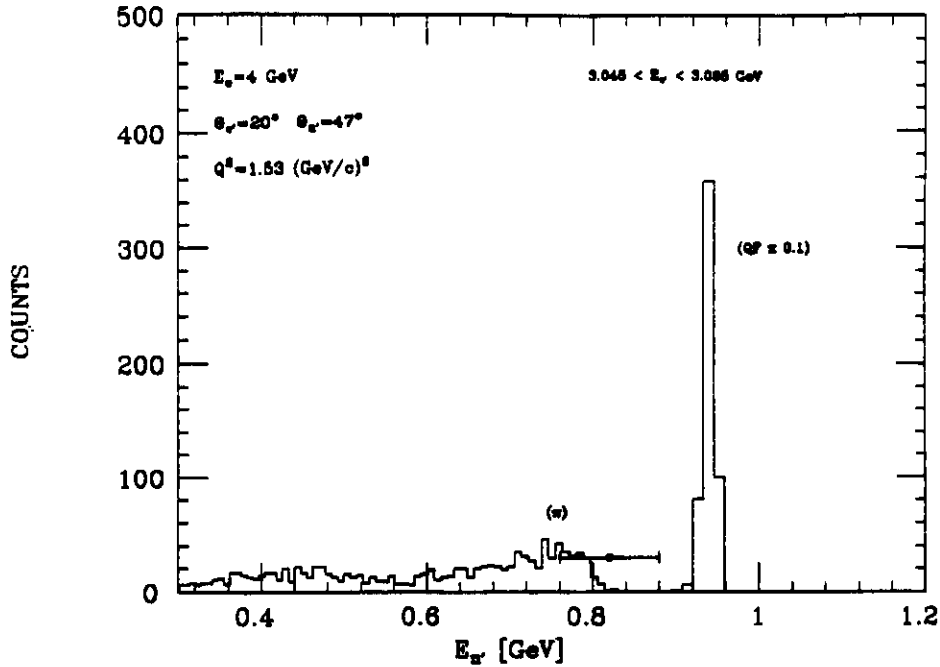


Figure 9: Neutron energy spectrum for electrons of $3.045 \leq E \leq 3.065$.

electron energy that selects 2/3 of the deuterium quasielastic peak (shown as the vertical dot-dash lines in Figures 10 and 11) has a contamination of 50% from $N(e, e')$ under the peak. The shape of $^{14}\text{N}(e, e')$ under the deuteron quasielastic peak need not be measured separately. The asymmetry measurement results in an increased counting rate for particular spin orientation of target and beam. The effect of the nitrogen contamination is a requirement to take better statistics.

We have made the estimate above using the inclusive (e, e') system only. When cutting events on the detection of the recoil neutron, (see Figure 11) the ^{14}N contribution is reduced by an additional factor such that it constitutes 25% at low Q^2 to less than 35% at high momentum transfers.

In the ND_3 target the ^{14}N also will be partially polarized. The unpaired neutron in ^{14}N also will contribute to the asymmetry. The ^{14}N quasielastic peak will show an asymmetry. Following the analysis of the EMC experiment[10], we estimate that this will constitute a 5% correction to the experimental asymmetry. This effect introduced by the ^{14}N can be measured directly by measuring the asymmetry in the wings of the ^{14}N quasielastic peak, whose shape is known from scattering from any ^{14}N target. This works because the asymmetry should be constant across the quasielastic peak and any corrections should be calculable.

As an additional check we are investigating the possibility of depolarizing the nitrogen by saturation with microwave power at very low temperatures as has been described in Ref. 11. This would allow actual measurements to be made at very low currents to confirm the nitrogen asymmetry contribution.

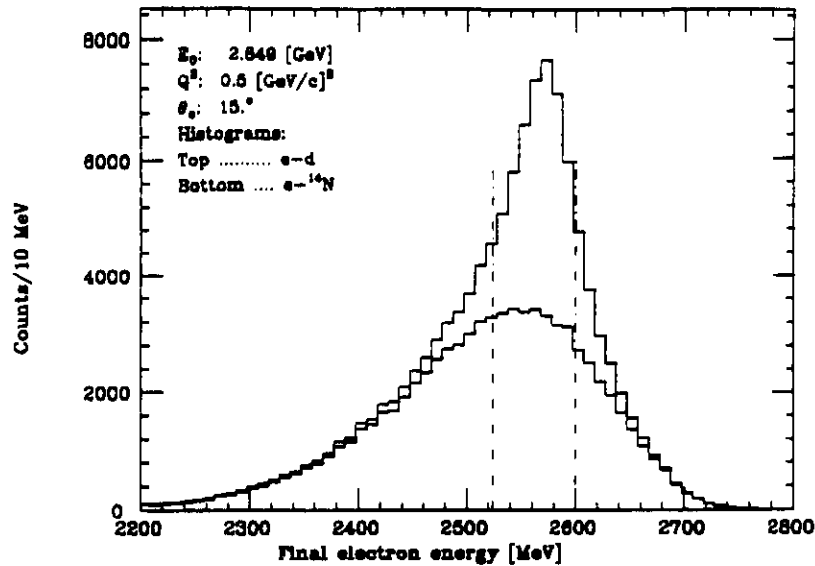


Figure 10: Inclusive quasielastic electron spectrum showing the narrow quasielastic deuteron peak on top of the much broader quasielastic nitrogen peak. The vertical dash-dot lines indicate the region of the spectrum which would be used to determine the asymmetry.

5.2 Charge exchange reactions

Not all events identified as a coincidence between an electron and a neutron necessarily correspond to the $(e, e'n)$ process. The reaction $(e, e'p)$, followed by charge exchange (p, n) can produce events of similar signature.

Two types of charge exchange processes occur:

- Charge exchange within the nucleus that produced the $(e, e'p)$ reaction
- Charge exchange in the rest of the target.

The former process cannot be distinguished experimentally from $(e, e'n)$. For the special case of the deuteron, the contribution of their process can be calculated accurately, and already is included in Arenhovel's calculation of FSI. It's effect is very small. Charge exchange in the ND_3 -target falls under two categories:

- $(e, e'p)$ on nitrogen, followed by (p, n) on nitrogen or deuterium. These events have the $(e - n)$ energy and angle correlation of quasielastic scattering from nitrogen. They are automatically subtracted out when removing the wide nitrogen quasielastic peak from the narrow deuteron quasielastic peak.
- $(e, e'p)$ on deuterium, following by (p, n) in ^{14}N or 2H . These events have the angular correlation of the genuine $(e, e'n)$ peak, and must be removed via a calculated correction.

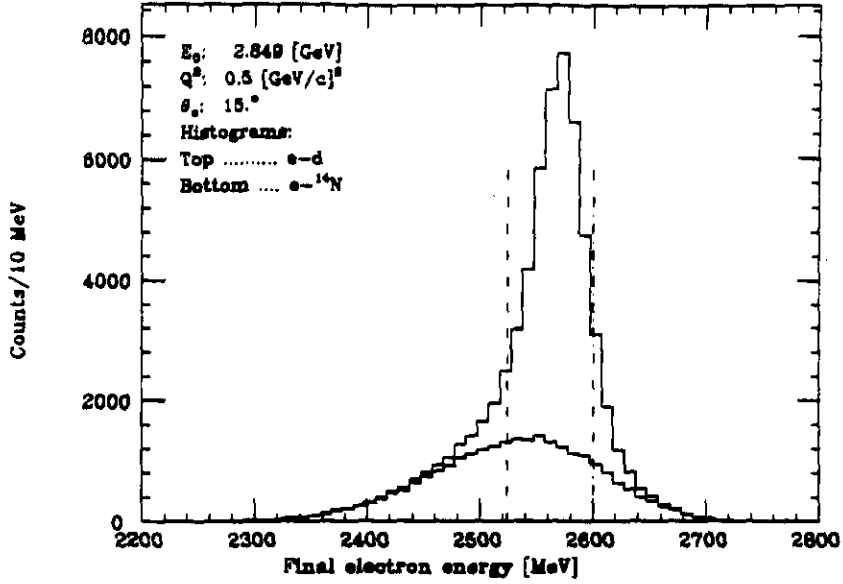


Figure 11: Electron Spectrum cut on detection of recoil neutron.

We have calculated their contribution to the measured asymmetry assuming a target thickness of about 1 g/cm^2 and using the known asymmetries for $(e, e'p)$ and cross sections, and measured (p, n) cross section at 0° . At $Q^2 = 0.5 \text{ GeV}^2/c^2$ (1.5) we find a relative change of A of 5.3×10^{-3} (3.5×10^{-3}), which is negligible in comparison with other systematic errors.

5.3 Uncertainties in $G_{Mn}(Q^2)$

All the presently proposed methods to determine G_{En} rely on a measurement of the interference term $G_{En} \cdot G_{Mn}$. From this term, G_{En} can be extracted to an accuracy that amounts at best to the one of our knowledge on $G_{Mn}(Q^2)$.

At the present time, the magnetic form factor G_{Mn} is known to an accuracy of typically 10%. While individual experiments have claimed significantly smaller uncertainties, the difference between experiments is of that order. This obviously could limit the accuracy of the G_{En} we wish to measure.

The present collaboration is actively involved in an experiment on $d(e, e'n)$ at NIKHEF (89-E2) and PSI that will improve the accuracy of G_{Mn} to the $\simeq 2\%$ level, for momentum transfers near 2 fm^{-1} . For the higher- q^2 region, this experiment will be extended as soon as the $\simeq 800 \text{ MeV}$ cw facilities at NIKHEF and Mainz will be operative. By the time G_{En} -data will be available, much more accurate G_{Mn} data will have been measured.

We note that these G_{Mn} experiments also provide the present collaboration with much experience on $(e, e'n)$ and the difficulties encountered with such detectors in the environment of an intense electron beam.

6 Estimate of Uncertainties

As it was mentioned earlier, the target asymmetry A_{ed}^V is related to the experimental asymmetry through

$$A_{ed}^V = \frac{\varepsilon}{p_b P_t}; \quad (p_b = p_{beam}, \quad P_t = P_d^1). \quad (8)$$

The uncertainty δA_{ed}^V can therefore be expressed as

$$\left(\frac{\delta A_{ed}^V}{A_{ed}^V}\right)^2 = \left(\frac{\delta \varepsilon}{\varepsilon}\right)^2 + \left(\frac{\delta p_b}{p_b}\right)^2 + \left(\frac{\delta P_t}{P_t}\right)^2, \quad (9)$$

which is a valid expansion since these uncertainties are uncorrelated. From $\varepsilon = (N_+ - N_-)/(N_+ + N_-)$, one can obtain the exact expression $\delta \varepsilon = 2\sqrt{N_+ N_-}/(N_+ + N_-)^{3/2}$ which can be approximated as $\delta \varepsilon \cong 1/\sqrt{N}$, for the usual case of small ε (implying $N_+ \cong N_- \cong N/2$). Therefore

$$\left(\frac{\delta A_{ed}^V}{A_{ed}^V}\right)^2 = \frac{1}{(A_{ed}^V p_b P_t)^2 N} + \left(\frac{\delta p_b}{p_b}\right)^2 + \left(\frac{\delta P_t}{P_t}\right)^2. \quad (10)$$

It is expected that at CEBAF the beam polarization will be measured with an accuracy of better than 5%, as it has been done at other laboratories[11]. We expect the situation to improve such that we have used 3% in our estimates. The target polarization has been determined to $\pm 3\%$ in current designs.

In the case of ND_3 targets, the nitrogen also acquires a degree of polarization, so the experimental asymmetry becomes

$$\varepsilon = p_b P_t A_{ed}^V \left(\frac{1 + \alpha' \beta'}{1 + \beta'}\right), \quad (11)$$

where $\alpha' = P_N/P_D$ is the ratio of the neutron's polarization to the deuteron's, and $\beta' = d^3\sigma_{e-N}/d^3\sigma_{e-D} = f_N N_N/(N_{ND_3} - N_N)$ is the ratio of the nitrogen to deuterium cross sections, which can be expressed in terms of the number of counts for the ammonia target N_{ND_3} , the counts for nitrogen N_N and a normalization factor $f_N = \mathcal{L}_{D_3} t_{D_3}/(\mathcal{L}_N t_N)$, which combines the luminosities and counting times for each target. The asymmetry $A_n(\equiv A_{ed}^V)$ has been assumed to be the same for quasifree neutrons in either nuclei. The resulting correction factor has been estimated using expected values for α' and β' was computed from spectra similar to those shown in Figures 10 and 11 for each value of Q^2 . The magnitude of α' is estimated to be 50%, and β' ranges from $\simeq 0.18$ at low Q^2 to $\simeq 0.21$ at high momentum transfer, leading to correction factors of 0.94 to 0.91 for ε .

The resulting expression for δA_{ed}^V involves two additional terms, corresponding to the uncertainties in α' and β' . However, $\delta \alpha'$ is multiplied by a factor $(\partial A_{ed}^V/\partial \alpha')$ that reduces it to the order of 1%, and thus it can be neglected relative to the other

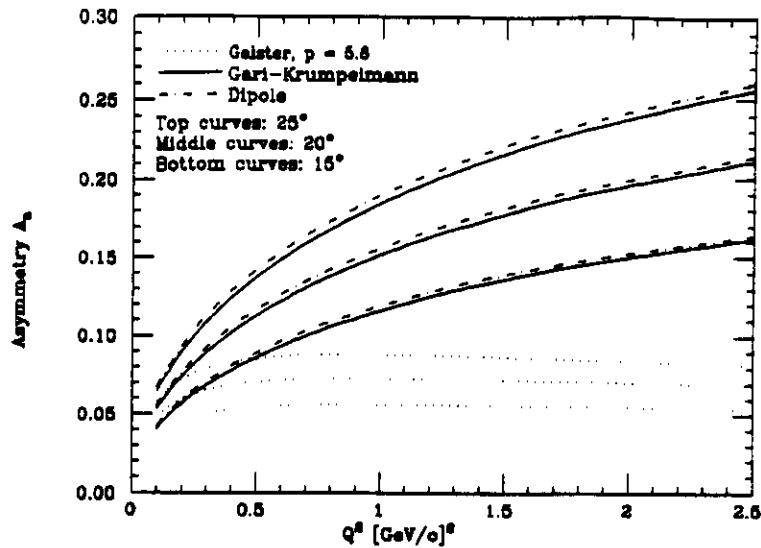


Figure 12: A_n as a function of Q^2 for three models and three angles.

terms. For β' , we find the usual $\approx 1/\sqrt{N}$ dependence, which in this case means $N = N_{ND_3}$ counts, resulting in $\delta\beta'/\beta' \leq 1\%$ as well, so the original expression for δA_{ed}^V remains valid.

The magnitude of δA_{ed}^V is determined by the requirement that it should allow to discriminate among the various models for G_{En} , and it has to be consistent with the lower limits imposed by the uncertainties $\delta p_b, \delta P_t$. Moreover, it should not represent an unreasonably large number of counts.

From Figure 12 it can be seen that to distinguish, for example, between the Galster parametrization and the Gari-Krumpelmann (G-K) model in the kinematic region of interest, δA_{ed}^V has to be of the order of $\sim 8 \times 10^{-3}$ at the low Q^2 points, to ~ 0.04 on the high momentum transfer side, for a four standard deviation (or better) separation between data points. On this basis, and taking as reference the G-K model, Table 3 illustrates the magnitude of the expected uncertainties in the asymmetry A_{ed}^V , the experimental asymmetry ϵ and the number of counts needed for the desired level of precision. (N.B. We have made these estimates for a fixed solid angle for the neutron detector. The situation may be improved if we allow that the neutron detector can be moved closer to the target at low Q^2 , thereby intercepting a greater fraction of the neutron quasielastic peak.)

In this table, the values of N were computed using the following additional assumptions: $p_b = 0.4 \pm 3\%$, $P_t = 0.5 \pm 3\%$. (It is clearly an advantage to work towards developing a low current source with $P_b \simeq 1$ for this experiment.) Moreover, we used the full expression for the experimental asymmetry, including corrections for the nitrogen contribution and its polarization, namely

$$\epsilon = \frac{N_+ - N_-}{N_+ + N_-} = \frac{(N_{ND_3}^+ - N_N^+) - (N_{ND_3}^- - N_N^-)}{(N_{ND_3}^+ - N_N^+) + (N_{ND_3}^- - N_N^-)}, \quad (12)$$

where the symbols have been defined earlier. The uncertainty in ε is then

$$\delta\varepsilon = \frac{2\sqrt{N^2\delta^2N_+ + N^2\delta^2N_-}}{(N_+ + N_-)^2}, \quad (13)$$

with the caveat that $\delta^2N_{\pm} = N_{ND_3}^{\pm} + N_N^{\pm}$, since the errors are additive. If we define $\alpha = N_N^-/N_N^+$, $\beta = N_N^+/N_{ND_3}^+$ and $\gamma = N_{ND_3}^-/N_{ND_3}^+$, we can express both ε and $\delta\varepsilon$ in terms of $N_{ND_3}^+$ alone, and since the asymmetry is always small, $N_{ND_3}^+ \cong N/2$, where N is the total required number of counts. The resulting expressions are

$$\varepsilon = \frac{1 - \beta - \gamma + \alpha\beta}{1 - \beta + \gamma - \alpha\beta} \quad (14)$$

and

$$N = \frac{8}{(\delta\varepsilon/\varepsilon)^2} \left[\frac{(\gamma - \alpha\beta)^2(1 + \beta) + (\gamma + \alpha\beta)(1 - \beta)^2}{(1 - \beta - \gamma + \alpha\beta)^2(1 - \beta + \gamma - \alpha\beta)^2} \right]. \quad (15)$$

Values for α, β and γ at each Q^2 were estimated from the same spectra used to compute β' , and using as reference the asymmetry predicted by the G-K model.

Table 3. Counts, FOM's and expected uncertainties

Q^2 [GeV/c] ²	θ_e	$\delta A_{ed}^V/A_{ed}^V$	$\delta\varepsilon/\varepsilon$	N	$\frac{FOM(Q^2)}{FOM(0.5)}$
0.5	15°	9.3%	8.2%	1.43×10^6	1
1.0	15°	12.9%	12.1%	5.53×10^5	0.23
1.5	20°	11.6%	10.8%	1.76×10^5	0.06
2.0	25°	12.3%	11.5%	8.2×10^4	0.02

This value for should be compared with the much simpler expression that is used when no contamination is present

$$N = \frac{1}{(p_b P_t A_{ed}^V \delta\varepsilon/\varepsilon)^2} \simeq \frac{1}{(p_b P_t \delta A_{ed}^V)^2}, \quad (16)$$

where the approximate equality obtains if we take $\delta A_{ed}^V/A_{ed}^V = \delta\varepsilon/\varepsilon$. We note that the minimum uncertainty in A_{ed}^V is restricted by the combined uncertainties in p_b, P_t , which in the present case amount to $\sim 4\%$.

To obtain G_{E_n} from the asymmetry, we have to solve the expression for A_{ed}^V (Equation 5) for the ratio G_{E_n}/G_{M_n} . Since the different models predict that as Q^2 increases, this ratio approaches and even exceeds 1 ($G_{E_n} = G_{M_n}$ at $Q^2 = 4m_n^2$ [GeV/c]² in the dipole and G-K models), it is inaccurate to neglect the term $(G_{E_n}/G_{M_n})^2$ in the Q^2 range of the present proposal. The result is that we have a quadratic equation for G_{E_n} that can be written as

$$\left(\frac{G_{E_n}}{G_{M_n}}\right)^2 + \frac{f(\tau, \theta_e)}{A_{ed}^V} \left(\frac{G_{E_n}}{G_{M_n}}\right) + g(\tau, \theta_e) = 0, \quad (17)$$

where $f(\tau, \theta_e) = 2\sqrt{\tau(1+\tau)} \tan(\theta_e/2)$, and $g(\tau, \theta_e) = \tau(1 + 2(1+\tau) \tan^2(\theta_e/2))$. The solutions are

$$G_{En} = \frac{-fG_{Mn}}{2A_{ed}^V} \left(1 \pm \sqrt{1 - 4g \left(\frac{A_{ed}^V}{f} \right)^2} \right). \quad (18)$$

By substituting in this expression the asymmetry predicted by a given model, it is seen that the negative root reproduces G_{En} . Therefore we can write

$$G_{En} = C(1 - R); \quad C = \frac{-fG_{Mn}}{2A_{ed}^V}, \quad R = \sqrt{1 - 4g \left(\frac{A_{ed}^V}{f} \right)^2}. \quad (19)$$

The purpose of this exercise is to obtain an expression for δG_{En} , based on the usual expansion for the uncertainties

$$\delta^2 G_{En} = \left(\frac{\partial G_{En}}{\partial G_{Mn}} \right)^2 \delta^2 G_{Mn} + \left(\frac{\partial G_{En}}{\partial A_{ed}^V} \right)^2 \delta^2 A_{ed}^V, \quad (20)$$

where the uncertainties $\delta\tau, \delta\theta_e$ have been neglected given their very small relative magnitudes.

After the appropriate substitutions are made, we find that

$$\left(\frac{\delta G_{En}}{G_{En}} \right)^2 = \left(\frac{\delta G_{Mn}}{G_{Mn}} \right)^2 + \left(\frac{\delta A_{ed}^V}{A_{ed}^V} \right)^2 C^2 \left(1 - \frac{1}{R} \right)^2 \frac{1}{G_{En}^2}. \quad (21)$$

This equation contains the effects of both the uncertainty in G_{Mn} as well as the propagation of the uncertainty in the asymmetry.

The table below shows that for the δA_{ed}^V considered earlier, there is a significant effect on G_{En} . The uncertainty in G_{Mn} was taken to be 5%, combining our present knowledge of this quantity at the Q^2 values of this proposal, with the precision expected from the ongoing measurements of G_{Mn} at NIKHEF-K and SLAC's NPAS experiment NE-11.

Table 4. Expected uncertainties in G_{En} ³

Q^2 [GeV/c] ²	θ_e	$\delta A_{ed}^V / A_{ed}^V$	$\delta G_{En} / G_{En}$	$\delta G_{En} / G_{En}^*$	$(\delta G_{En} / G_{En})^{Galster}$
0.5	15°	9.3%	12.9%	8.8%	16.8%
1.0	15°	12.9%	21.9%	12.5%	29.1%
1.5	20°	11.6%	24.8%	14.5%	30.3%
2.0	25°	12.3%	32.3%	18.2%	36.2%

³We have shown two values for $\delta G_{En} / G_{En}$ (based on G-K). The first set is for the conservative case of $p_b = 0.4$, the second (with an * for $p_b = 0.9$).

7 Count Rates and Beam Time Request

On the basis of the estimated numbers of counts presented in the previous section, we have computed the required counting times, displayed in the table below. To compute the rates, we have substituted in the expression for R ,

$$R = \frac{d^3\sigma}{d\Omega_e dE' d\Omega_n} \Delta\Omega_e \Delta E' \Delta\Omega_n \mathcal{L} \eta, \quad (22)$$

values for $d^3\sigma/(d\Omega_e dE' d\Omega_n)$ computed for the case of quasifree neutrons ($\vec{p}_n = \vec{q}$), as discussed in the works of Arenhövel *et al.*[5], Cheung and Woloshyn[12], Donnelly and Raskin[3], and Dmitrasinovic and Gross[13].

The additional factors in R are:

- $\Delta\Omega_e = 6.4$ [msr], for the Hall C High Momentum Spectrometer.
- $\Delta\Omega_n \geq 48$ [msr], for a 3 m by 1.5 m neutron detector placed at 10 m or less from the target (10 m for $Q^2 \geq 1.5[\text{GeV}/c]^2$).
- $\Delta E' \simeq 120$ [MeV], corresponding to about $\pm 2\%$ of the central momentum of the electron spectrometer.
- \mathcal{L} (luminosity) = 5.6×10^{33} , for a 10 nA current, equivalent to 6.2×10^{10} electrons/s, and a target density of $9 \times 10^{22}[\text{cm}^{-2}]$ polarizable neutrons for a 1.5 cm long target.
- $\eta \geq 30\%$, the neutron detector efficiency (30% at $Q^2 \geq 1.5\text{GeV}/c^2$).

Table 5. Counting rates and times

Q^2 [GeV/c] ²	N $\times 10^5$	$d^3\sigma$ $\frac{\text{nb}}{\text{sr}^2 \text{MeV}}$	R Hz	t hours	$\Delta k'(\pm 2\%)$ [MeV/c]	E' [GeV]
0.5	14.3	80.8	4.3	92.5	103	2.576
1.0	5.53	22.6	1.55	99.0	133	3.327
1.5	3.06	5.6	0.36	235.2	125	3.130
2.0	1.50	1.75	0.10	400.0	115	2.878

In addition, we plan to take measurements on NH_3 and N_2 targets, to measure G_{Ep} and to correct for backgrounds and systematic effects. The time requirements for these are as follows:

NH_3 : since the hydrogen polarization $P_H \geq 0.8$, the number of counts needed would be 4 times smaller. Furthermore, the cross section for $e-p$ scattering is 2.5 to 3.5 times larger than for $e-n$ reactions, so the the counting times are reduced by a combined factor of ~ 14 at low Q^2 to ~ 10 at high momentum transfer. Moreover, it should be mentioned that a higher beam current (~ 100 nA) may be used, since the NH_3 target can achieve its rated polarization at higher temperatures. In summary,

a request for beam time for the G_{E_p} measurement equal to 20% of the G_{E_n} time is being made.

N_2 : The measurements on a nitrogen target will be used to extract the backgrounds from the total quasielastic peaks, determining in this way the ratio $\beta = N_N/N_{ND_3}$, discussed earlier, in a model independent way. From the ratios of numbers of counts N_N and N_{ND_3} , used in the previous section, we would require 50 hours of beam time at significantly higher currents for this measurement.

Considerable time will be spent in beam polarization studies. The destructive Möller scattering technique does not allow data taking during polarization monitoring. To determine the beam polarization to 3% over long periods will require many short measurements. These hours are lumped together with target maintenance and calibration in the category of contingency for the experiment.

Summary of request

Data taking	825 hours
NH_3 runs	110 hours
N_2 runs	<u>50 hours</u>
Subtotal	995 hours
Contingency(1/3)	<u>330 hours</u>
Total	1325 hours

8 Commitments of Participants

The University of Virginia together with support from the University of Basel will assume the responsibility for the design and construction of the polarized targets and the neutron detector. The target is expected to require 1.1M\$ of equipment. Approximately one-half of the required neutron detector is being assembled at Virginia for initial experiments at the LEGS facility at Brookhaven. An additional \$300,000 will be required. The University of Virginia has supplied \$125,000 towards equipment for the target and a request has been made for an additional \$200,000 over the next two years. The University of Virginia will supply 9 FTE, including a senior physicist, to complete the target construction.

The University of Basel will contribute \$100,000 to the project.

9 References

1. A. Amroun *et al.* Saclay preprint.
2. Norman Dombey, Rev. Mod. Phys **41** (1969) 236.
3. T.W. Donnelly and A.S. Raskin, Ann. Phys. (New York) **169** (1986) 247, T.W. Donnelly and A.S. Raskin, Ann.Phys. (New York) **191**(1989) 81.
4. R.G. Arnold, C.E. Carlson and F. Gross, Phys. Rev. **C23** (1981) 363.
5. H. Arenhövel, W. Leidemann and E.L. Tomusiak, Z. Phys. **A331** (1988) 123.

6. S. Galster et al. Nucl. Phys. **B32** (1971) 221.
7. M. Gari and W. Krümpelmann, Z. Phys. **A322** (1985) 689, Phys. Lett. **B173** (1986) 10.
8. E. Schilling, Proceedings CEBAF 1986 Summer Workshop.
9. M. Placidi, V. Burkert, and R. Rossmanith, CEBAF-PR-89-010.
10. J. Ashman *et al.*, EMC preprint, CERN-EP/89-73, submitted to Nuclear Physics B.
11. G. R. Court and W. G. Heyes, NIM **A243** (1986) 37 - 40, G. R. Court, W. G. Heyes, W. Meyer, and W. Thiel, in Proceedings of the Fourth International Workshop on Polarized Target Materials and Techniques, Bonn, W. Meyer, Editor, 1984.
12. C. Y. Cheung and R. M. Woloshyn, Phys. Lett. **B127** (1983) 147.
13. V. Dmitrasinovic and F. Gross, *Polarization Observables in Deuteron Photo- and Electro- Disintegration*, CEBAF-PR-89-022.